1977), vols. 1 and 2; S. L. Holt, *J. Dispersion Sci. Technol.* **1**, 423 (1980); H.-F. Eicke, *Top. Curr. Chem.* **87**, 85 (1980).
12. On the structural properties of protein-containing micelles see F. J. Bonner, R. Wolf, P. L. Luisi, *J. Solid-Phase Biochem.* **5**, 255 (1980); A. V. Levashov, Yu. L. Khmelnitsky, N. L. Klyachko, V. Ya. Chernyak, K. Martinek, *Anal. Biochem.* **118**, 42 (1981); *J. Colloid Interface Sci.* **88**, 444 (1982).
13. "Novel lipidic particles" similar to reverse micelles sandwiched between the monolayers of the lipid bilayer in biological membranes have been discovered. See B. de Kruijff *et al.*, in *International Cell Biology 1980–1981*, H. G. Schweiger, Ed. (Springer, Berlin, 1981), p. 559; A. J. Verkleij and B. de Kruijff, *Nature (London)* **290**, 427 (1981).
14. An optimal concentration of water in micelles has been demonstrated for α-chymotrypsin (*5, 8*), pyrophosphatase (*5*), and liver alcohol dehydrogenase (*8*). Furthermore, by using different micelle-forming surfactants such as Aerosol OT, Twin-20, Triton X-45, and Cetyltrimethylammonium bromide (CTAB), Eremin *et al.* (*9*) found conditions under which cytochrome P-450 (form LM-2, which is unstable in buffer solution) has the same "lifetime" as in microsomes.
15. K. Martinek, Yu. L. Khmelnitsky, A. V. Levashov, I. V. Berezin, *Dokl. Akad. Nauk SSSR* **263**, 737 (1982).
16. K. Martinek, N. L. Klyachko, A. V. Levashov, I. V. Berezin, *ibid.*, in press.
17. The polarity, dielectric permeability, and local viscosity of the micelle interior and the reactivity of micelle-solubilized water molecules are very different from those of bulk water (*11*). Moreover, a pK_a shift of active site functional groups of micelle-entrapped enzymes was observed (*5, 6, 8*). A spin probe on an α-chymotrypsin active site showed restricted rotational freedom (G. I. Lichtenstein *et al.*, *Biokhimia*, in press).
18. The occurrence of conformational changes in the structure of micelle-entrapped protein is supported by ultraviolet and circular dichroism spectral data (*8, 16*). The alterations in the protein conformation may be due to microenvironmental effects and direct interactions between the protein and surfactant molecules, as is frequently the case in aqueous solutions [C. Tanford, *Adv. Protein Chem.* **23**, 121 (1968); J. Steinhardt and J. A. Reynolds, *Multiple Equilibria in Proteins* (Academic Press, New York, 1969); S. Lapanje, *Physico-chemical Aspects of Protein Denaturation* (Wiley, New York, 1978); E. Mori and B. Jirgensons, *Biochemistry* **20**, 1630 (1981)].
19. The kinetic role of the partition effect has been analyzed theoretically and demonstrated experimentally (*5*).
20. For examples, see E. Antonini, G. Carrea, P. Cremonesi, *Enzyme Microb. Technol.* **3**, 291 (1981); K. Martinek and A. N. Semenov, *J. Appl. Biochem.* **3**, 93 (1981); M. D. Lilly, *J. Chem. Technol. Biotechnol.* **32**, 162 (1982).

25 January 1982; revised 28 May 1982

Neuromagnetic Localization of Epileptiform Spike Activity in the Human Brain

Abstract. *Local paroxysmal discharges of epileptic tissue within the human brain, which may be electrically recorded as voltage spikes in the electroencephalogram, also generate extracranial magnetic fields. These fields were assessed by means of recently developed neuromagnetometric techniques. Surface measurements of magnetic spike field strength in the region of the focus appear sufficient to establish the location, depth, orientation, and polarity of currents underlying the paroxysmal discharge.*

Most living cells maintain an electrical potential across their outer membrane; in the nervous system, it is this feature of the neuron that provides the basis for electrical signaling. When similar patterns of electrical activity are occurring in populations of cortical neurons, electrical potentials reflecting this activity may be recorded from the scalp (*1*). Under many conditions these same currents also generate extracranial magnetic fields (*2*). Synchronous firing of regional neuronal populations often occurs in healthy brain, the response to sensory stimulation being one common example (*3*). However, synchronous firing also marks certain neuropathologies, in particular the epilepsies (*4*). We now report that the measurement of extracranial magnetic fields produced by abnormal discharge in limited regions of the human cortex provides precise spatial information concerning the location, depth, and orientation of currents within the epileptogenic focus.

Focal (partial) epilepsy is a disorder characterized by the disposition of restricted regions of the cortex toward the production of synchronous paroxysmal discharges (*5*). Occasionally, this activity may spread beyond its normal boundaries to include larger areas of cortical tissue, resulting in a clinical seizure, or ictus. Between such ictal episodes, the epileptic focus often produces single, randomly occurring paroxysmal transients, termed interictal spikes. Interictal spikes may be recorded electrically over wide regions of the scalp, but precise electrical localization often requires recording from arrays of electrodes surgically placed on the cortical surface or implanted in the depth of the brain (*5, 6*).

Interictal spikes may be expected to be more sharply localized in the magnetoencephalogram (MEG) than in its electrical counterpart, the electroencephalogram (EEG), for several reasons. First, the magnetic field is influenced primarily by intracellular axial currents, which are confined to the region of the discharging cortex; the EEG, in contrast, is dominated by volume currents, which distribute the electrical potential throughout wide areas of bodily tissue (*2*). Second, the electrically resistive skull is transparent with respect to brain magnetic fields, whereas it distorts and smears volume-conducted brain electrical potentials (*2, 7*). For this reason, MEG recordings have been shown to have a spatial resolution more similar to electrical recordings made directly from the surface of the brain than to that of the scalp EEG (*3, 8*). Finally, MEG is an absolute rather than differential measure. Spatial derivatives of the magnetic field may be determined by comparing flux strength proximal to the scalp with that of a distal point on the same axis, unlike the EEG which requires reference to a secondary scalp location (*9*).

Neuromagnetic measurements were obtained from one child and one adult with focal (partial) seizure disorders (*10*). Previous examination of the scalp EEG for subject 1 revealed right temporofrontal (Sylvian) spike discharges; for subject 2 the discharge was in the left anterior temporal region. A dependent contralateral homologous EEG spike focus was also recorded in subject 1.

Brain magnetic fields were measured normal to the scalp in an unshielded environment by using a superconducting quantum interference device (SQUID) coupled to a second-derivative flux transporter with a coil diameter of 2.4 cm and separation of 3.2 cm. The probe assembly consisting of the SQUID and gradiometer was mounted in a fiberglass Dewar containing liquid helium (*11*). The lowest coil of the gradiometer was positioned tangentially 17 mm above the scalp over a rectangular matrix of 28 closely spaced points (2 cm), centered on the approximate EEG spike focus. For each point in the matrix, at least ten interictal spikes were recorded magnetically. During all magnetic measurements, concurrent EEG was recorded bilaterally from temporal electrodes in a bipolar configuration (*12*). Both the one channel of MEG and the six channels of EEG were amplified (Grass model 8-18 C electroencephalograph), band-pass filtered (MEG: 1 to 35 Hz; EEG: 1 to 70 Hz, −3 dB), and digitized on-line (PDP 11/34). Eight-second samples containing the magnetic and electrical spike activity were stored digitally on magnetic tape for further analysis. The principal features of the magnetic data were replicated on a separate occasion for each patient. During every recording session, magnetic measurements were also performed with the probe removed from the subject's head to control for environmental artifacts.

Data analysis was performed in three phases. First, the sampled MEG and EEG data were displayed in 8-second blocks on a high-resolution storage CRT display (Tektronix 611). The EEG was

0036-8075/82/1126-0891$01.00/0

scanned by means of a multichannel electronic cursor to time mark the crest of EEG spikes in the primary focus. Next, by using these visually identified markers, separate 1-second averages were made of the MEG and EEG channels over 10 to 15 consecutive spikes for each MEG measurement point. Finally, isocontour plots were constructed, displaying the amplitude and polarity distribution of selected components of the average magnetic spike across the measurement matrix (*13*). Magnetic field extrema were then determined, from which the three-dimensional location of the component generators was calculated (*9*).

Figure 1A shows the rectangular MEG recording matrix (8 by 14 cm) positioned over point T4 in the right temporal area of subject 1. Average magnetic traces for each of the points within the matrix are displayed in Fig. 1B. The amplitude and polarity of the magnetic spike demonstrates an orderly spatial distribution throughout the matrix. Figure 1F shows enlargements of traces from two points where the magnetic spike is at its maximum. The morphology of the magnetic spike is quite similar to that of the EEG

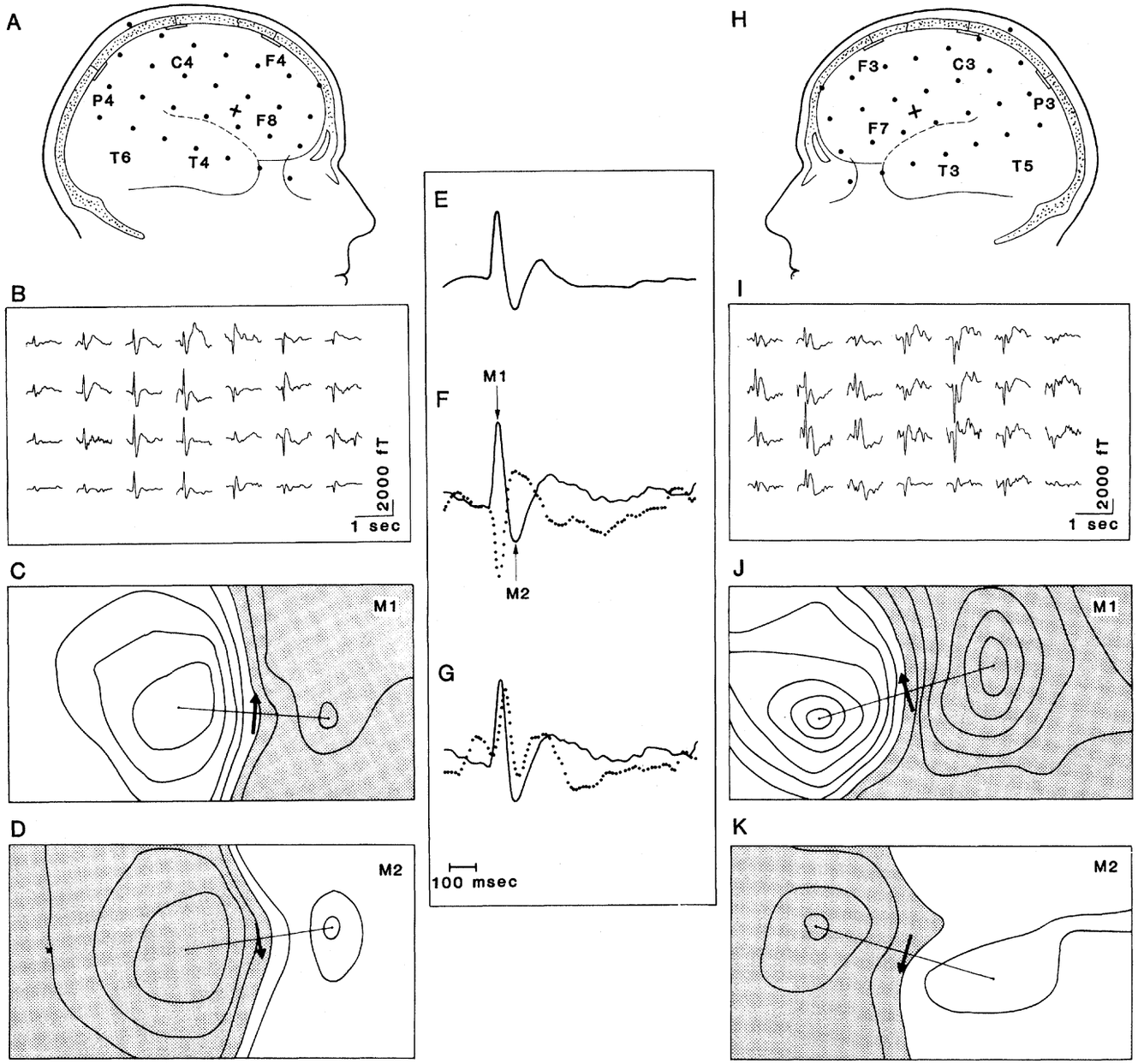

Fig. 1. Averaged magnetic spike activity measured from the right and left hemispheres of subject 1. (A) and (H) Rectangular MEG measurement matrices (2-cm spacing) oriented along the temporal axes of both hemispheres. Crosses mark the location of MEG spike foci. (B) and (I) Average magnetic spikes for each point within the right and left hemisphere MEG matrices. (E) Average EEG spike recorded from the T4-T6 derivation over the right hemisphere (90 μV baseline to peak, T4 negative up; negative spike phase reversed at T4-F8). (F) Enlargement of two average traces near the extrema of the magnetic fields from the left area (solid line) and right area (dotted line) of the right hemisphere MEG matrix, demonstrating two reliable temporal components (M1 and M2) and the opposing polarity reflecting the magnetic field simultaneously leaving (up) and entering (down) the cortex. (G) Magnetic spike from the left hemisphere (dotted line, rescaled for comparison) is delayed by 20 msec when compared to that of the right (solid line). (C) and (D) Isocontour plots demonstrating the amplitude [750 femtoteslas (fT) per bar] and polarity (light indicates emerging, and shaded, reentering) distribution of magnetic fields associated with M1 and M2 of the right hemisphere. Straight lines connecting the field extrema demark the orientation of the magnetic fields. Arrows represent the location and polarity of underlying current sources. (J) and (K) Similar contour plots displaying magnetic field distributions of M1 and M2 over the left hemispheric focus.

spike (Fig. 1E) averaged from the primary EEG focus of the right hemisphere. The two MEG traces (solid and dotted lines) are mirror images, representing magnetic field extrema, where the magnetic field simultaneously leaves and enters the head. This field pattern indicates that the underlying neural generators may be represented as a simple dipolar current source (9). The direction of field circulation reverses several times, reflecting polarity reversals of the current dipole. This magnetic spike complex has two reliable temporal components, the magnetic spike itself (M1) and a subsequent sharp wave (M2). Two later slow waves may also be discerned; however, their appearance is not consistent throughout the measurement matrix.

Separate isocontour plots constructed for each of the magnetic components more clearly display their field distributions (Fig. 1, C and D). Magnetic field extrema are present in both plots. Lines have been drawn connecting these extrema to indicate the orientation of the magnetic fields. Bisecting these is an orthogonal arrow showing the position and polarity of the putative current dipoles that give rise to the magnetic fields (9). Their locations within the matrices are very similar, suggesting a common generator in the right fronto-opercular region (cross on Fig. 1A) for both M1 and M2.

If one assumes that the active cortical region responsible for the interictal spike can be represented as a current dipole, its depth may also be calculated. The depth measurement is determined from the angle indicated by the two field extrema with respect to the center of a sphere modeling the cranium (9). Because the skull is not perfectly spherical, an approximate model was derived by using the diameter between the surface location of the dipole and a homologous point on the contralateral side, and the coronal half-circumference between these same two points. The resultant calculations were adjusted for the added distance between the scalp and the lower gradiometer coil. This yielded a depth below the scalp of 10 mm for M1 and 11 mm for M2, again suggesting a common current source for both components near the lateral surface of the right frontal operculum.

Figure 1H shows the MEG measurement matrix over the contralateral secondary focus within the left hemisphere of subject 1. The spatial distribution of the magnetic spike discharges, averaged with reference to the same EEG spike as was used for the contralateral side, displays an equally well-defined anterior-posterior polarity reversal (Fig. 1I). Figure 1G shows that the morphology of M1 and M2 of the secondary left hemisphere magnetic spike (dotted line) closely matched that of the right (solid line), although the signal was systematically delayed by 20 msec. This delay probably reflects the dependence of the left hemisphere focus on transcollosal discharge from the right. Contour plots reveal clear field extrema for both components of the left-hemisphere magnetic spike complex (Fig. 1, J and K). Again, the restricted and consistent magnetic field pattern of both components suggests a common generator in the fronto-opercular region of the cortex (cross on Fig. 1H) for both M1 and M2. The depths of the current sources beneath the scalp were calculated to be 16 and 17 mm, respectively. Perhaps the most striking feature of these plots is their similarity in every dimension to those of the contralateral hemisphere.

The second subject showed electroencephalographic indications of focal activity in the anterior temporal cortex of the left hemisphere. Therefore, the 14 by 8 cm recording matrix used with subject 2 was positioned over point T3 in the left temporal area (Fig. 2A). Recording and analysis procedures were as described previously. For this subject the average magnetic spike displayed a polarity reversal along the vertical axis (Fig. 2B). The morphology of the magnetic spike was similar to that of subject 1 with two consistent temporal components. Isocontour plots for each of these components showed clear field extrema (Fig. 2, C and D). Calculation of depth and position indicated that these components were produced by a common generator that may be modeled by a current dipole approximately 10 mm below the scalp in the left anterolateral temporal lobe (cross on Fig. 2A).

In both subjects, the magnetic field produced by the interictal spike was consistent with the focal nature of their epileptic disorders. Furthermore, magnetic field mapping provided a unique and consistent physiological indication of the position and depth of the epileptogenic focus. The close similarity in the localization of the bilateral foci of subject 1 demonstrates the precision not only of transcollosal connections but also of the neuromagnetic recording technique. In both subjects, the current source for the magnetic spike was determined to be superficial, near the lateral surface of the cortex. However, other

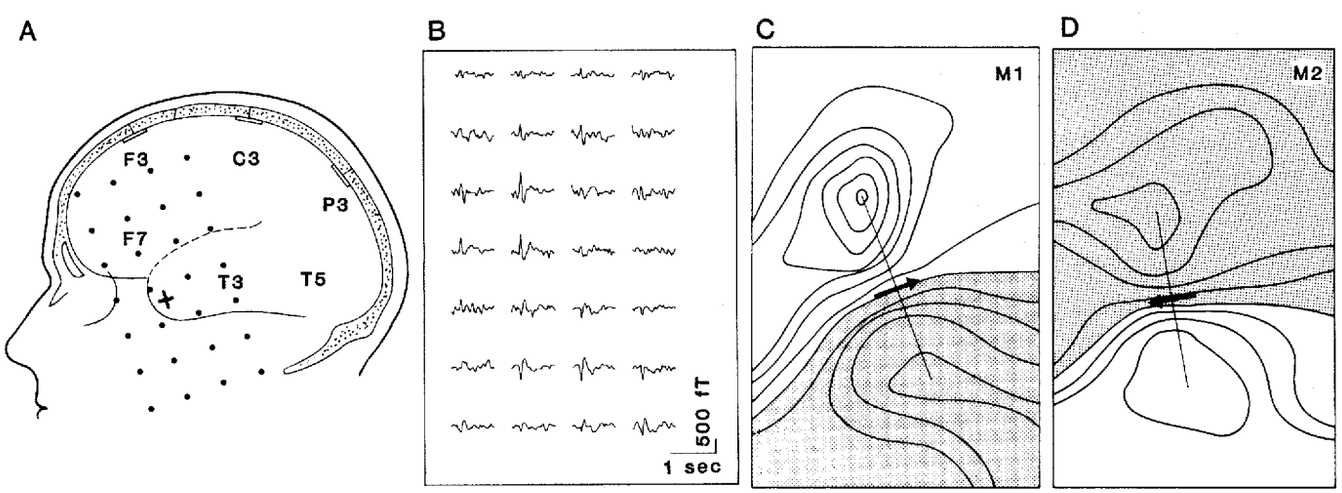

Fig. 2. Average magnetic spike activity measured from the left hemisphere of subject 2. (A) Rectangular MEG measurement matrix covering the left anterior temporal region. A cross marks the spot of the MEG spike focus. (B) Average magnetic spikes obtained from each point in the matrix. (C) and (D) Isocontour plots (similar to those in Fig. 1) displaying the amplitude and polarity distributions of the generators of M1 and M2. The EEG spike was similar in morphology to the MEG spike and was maximal at T1, below and posterior to F7.

data from our laboratory indicate that deeper, more mesial discharges may also be recorded neuromagnetically.

These results demonstrate that by neuromagnetic mapping of interictal spikes in the human brain it is possible to identify with precision the three-dimensional location of intracortical sources producing epileptiform discharges. Further analyses of the orientation, polarity, and timing of these fields, coupled with detailed postsurgical histological data, may provide insight about rapidly occurring cellular events underlying interictal spiking.

DANIEL S. BARTH
Department of Psychology, University of California, Los Angeles 90024
WILLIAM SUTHERLING
JEROME ENGEL, JR.
Department of Neurology, University of California, Los Angeles 90024
JACKSON BEATTY
Department of Psychology, University of California, Los Angeles 90024

References and Notes

1. O. D. Creutzfeldt, in *Basic Mechanisms of the Epilepsies*, H. H. Jasper, A. A. Ward Jr., A. Pope, Eds. (Little, Brown, Boston, 1969) pp. 397–410; D. A. Pollen, in *ibid.*, pp. 411–420.
2. S. J. Williamson and L. Kaufman, *J. Magn. Magn. Mat.* **22**, 129 (1981).
3. W. R. Goff, T. Allison, H. E. Vaughan, Jr., in *Event Related Potentials in Man*, E. Callaway and S. H. Koslow, Eds. (Academic Press, New York, 1980), pp. 1–81.
4. Both electrical and magnetic recordings of epileptiform activity have been previously reported [J. Scheurer and J. Calvet, in *Synchronization of EEG Activity in the Epilepsies*, H. Petsche and M. A. B. Brazier, Eds. (Springer-Verlag, New York, 1972); D. Cohen, *Science* **175**, 664 (1972); J. R. Hughes, J. Cohen, C. I. Mayman, M. L. Scholl, D. E. Hendrix, *J. Neurol.* **217**, 79 (1977); G. B. Ricci, G. L. Romani, I. Modena, S. Barbanera, R. Leoni, P. Carelli, *Electroencephalogr. Clin. Neurophysiol.* **52**, S95 (1981)].
5. W. Penfield and H. H. Jasper, *Epilepsy and the Functional Neuroanatomy of the Human Brain* (Little, Brown, Boston, 1954); F. A. Gibbs, E. L. Gibbs, W. G. Lennox, *Brain* **60**, 377 (1937); T. A. Pedley, *Ann. Neurol.* **3**, 2 (1978).
6. C. Ajmone-Marsan, in *Electrodiagnosis in Clinical Neurology*, M. J. Aminoff, Ed. (Churchill Livingstone, New York, 1980), pp. 167–196; J. Bancaud, in *Handbook of Electroencephalography and Clinical Neurophysiology*, A. Rémond, Ed. (Elsevier, Amsterdam, 1975), vol. 10, part B; P. Gloor, *Adv. Neurol.* **8**, 59 (1975); J. Engel, Jr., P. H. Crandall, R. Rausch, in *The Clinical Neurosciences*, R. N. Rosenberg *et al.*, Eds. (Churchill Livingstone, New York, in press).
7. P. L. Nunez, *Electric Fields of the Brain: The Neurophysics of EEG* (Oxford Univ. Press, New York, 1981).
8. D. Brenner, S. J. Williamson, L. Kaufman, *Science* **190**, 480 (1975); D. Brenner, J. Lipton, L. Kaufman, S. J. Williamson, *ibid.* **199**, 81 (1978); G. L. Romani, S. J. Williamson, L. Kaufman, *ibid.* **216**, 1339 (1982).
9. S. J. Williamson and L. Kaufman, in *Biomagnetism*, S. N. Erne, H. D. Hahlbohm, H. Lübbig, Eds. (de Gruyter, Berlin, 1981), pp. 353–402.
10. Subject 1 was a 10-year-old female of normal intelligence with no family history of epilepsy. Focal left facial clonic (partial motor) seizures began at age 9. These occasionally generalized into grand mal (generalized tonic-clonic) seizures. At the time of testing she was receiving carbamazepine (Tegretol) with resulting control of seizures. Subject 2 was a 37-year-old female with recent memory deficits and no family history of epilepsy. Her grand mal (generalized tonic-clonic) and psychomotor (complex partial) seizures began at 19 years of age when she had toxemia. At the time of testing she was receiving phenobarbital and experiencing weekly partial complex seizures and, more rarely, generalized seizures.
11. S.H.E. Corporation, San Diego, California.
12. Standard electrode positions were used depending on the side and location of the focus. Subject 1: FP2-F8, F8-T4, T4-T6, T6-O2, FP1-F7, F7-T3. Subject 2: FP1-T1, T1-T3, T3-T5, T5-O1, FP2-T2, T2-T4. These positions were selected according to the established International 10-20 System [H. H. Jasper, *Electroencephalogr. Clin. Neurophysiol.* **10**, 371 (1958)]. Abbreviations: T, temporal lobe; F, frontal lobe; FP, frontal pole; O, occipital lobe. Odd numbers indicate standard positions over the left hemisphere, and even numbers, over the right hemisphere.
13. D. Lehmann, in *EEG Informatics. A Diadactic Review of Methods and Applications of EEG Data Processing*, A. Rémond, Ed. (Elsevier, New York, 1977), pp. 365–385.
14. This research was supported in part by the Environmental Physiology Program of the Office of Naval Research on Contract N00014-76-C-0616, by USPHS grant 5-S07 RR07009, and by NIMH training grant 78040-29867-5. We thank J. Perry Jaster for his expertise and assistance in the construction of equipment for this project.

6 July 1982; revised 23 August 1982

Stimulation of Feeding in Rats by Intraperitoneal Injection of Antibodies to Glucagon

Abstract. *Intraperitoneal injections of antibodies to pancreatic glucagon at the onset of the first meal after 12 hours of food deprivation increased meal size 63 percent and meal duration 74 percent in rats. The antibodies also reduced the increase in hepatic vein blood glucose that occurred during meals in control rats, but did not affect the prandial increase in portal vein blood glucose. These results suggest that, under these conditions, pancreatic glucagon is necessary for the normal termination of meals.*

The observation that glucagon injections inhibit feeding in several species (*1–8*) suggests that this hormone, in addition to having extensive metabolic functions (*9*), may be involved in the neuroendocrine control of the behavioral processes that end meals. In rats, glucagon injections that produce glycemic changes in the normal prandial range reduce meal size and duration but do not disrupt the normal behavioral sequence characterizing postprandial satiety (*2, 3*). Glucagon's inhibitory effect is specific for feeding because neither water intake nor body temperature is affected and because no behavioral signs of malaise or aversion are produced (*3, 4*). Exogenous glucagon therefore fulfills the behavioral criteria for a putative endocrine satiety signal (*10*).

The possibility that endogenous glucagon is a physiological satiety signal arises from the observation that plasma glucagon concentrations increase during consumption of mixed-nutrient meals (*11*). If prandial increases in endogenous glucagon are necessary for normal satiety, partial inactivation of circulating glucagon should release feeding from inhibition. We tested this by injecting rats with antibodies to glucagon at the onset of meals. Such injections increased both meal size and length.

Individually caged male Sprague-Dawley rats (260 to 340 g) were maintained for at least 2 weeks on a reversed 12-hour light-dark cycle with unlimited access to a powdered high-carbohydrate diet (*12*). On the test day the rats were deprived of food during the light phase and offered preweighed cups of food at the beginning of the dark phase. One of

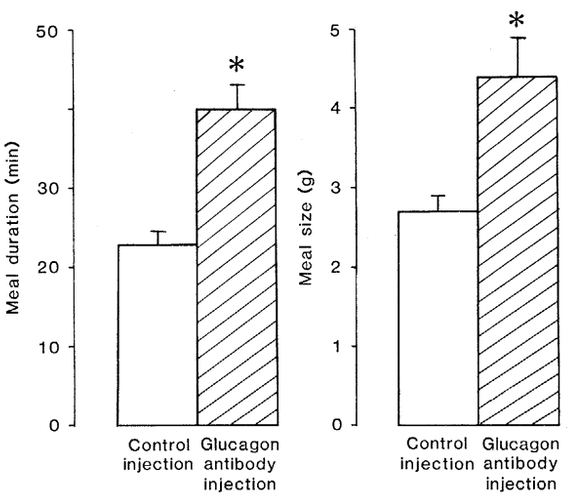

Fig. 1. Meal duration and size in rats deprived of food for 12 hours and injected at meal onset with glucagon antibodies ($N = 18$) or vehicle ($N = 28$). Data are means ± standard errors. Symbol: (*) $P < .002$.

0036-8075/82/1126-0894$01.00/0